energies

MDPI

Article

Dynamic Modelling and Experimental Validation of a Pneumatic Radial Piston Motor

Kyle Grimaldi, Ahmad Najjaran, Zhiwei Ma *, Huashan Bao and Tony Roskilly

Department of Engineering, Durham University, Durham DH1 3LE, UK
* Correspondence: zhiwei.ma@durham.ac.uk

Abstract: A pneumatic radial piston motor is studied in this paper in order to establish a dynamic modelling and simulation method. As a result of using geometric parameters, the piston cylinder volume change was calculated, and the heat transfer equation, thermodynamic energy balance equation, and motion equation were combined in order to create a complete model of the piston cylinder. With the aid of compressed air, several experimental tests were conducted, and the results of rotational speed with varying inlet pressure were fed into the simulation to determine one of the critical unknown parameters, such as the overall friction coefficient of the system. For the studied piston motor, this coefficient was 0.0625 Nm. Computer simulations can be used to adjust design parameters in order to reach a higher rotation speed by using an accurate model. As a result, better efficiency and performance present several opportunities that would not be possible when running experimental tests in a lab. The mathematical model yielded higher rotational speeds of 50 RPM on average, with an increased piston diameter of 1.775 mm; by increasing the diameter of the cylinder to 25.8 mm, it was possible to achieve faster rotational speeds. The performed precise simulation could be used for further motor design and optimisation, and performance estimates under a broader range of operational conditions. Simulations should be conducted on multiple sets of experimental test results to determine the correct f_{overall} value for each motor. In addition to guiding the design and optimisation of the motor, simulations could also predict its performance under a broader range of operating conditions by utilising effective parameters such as geometrical characteristics, flow conditions, and motion equations.

Keywords: pneumatic radial piston motor; modelling; experimental validation; overall friction coefficient; optimisation

Citation: Grimaldi, K.; Najjaran, A.; Ma, Z.; Bao, H.; Roskilly, T. Dynamic Modelling and Experimental Validation of a Pneumatic Radial Piston Motor. *Energies* **2023**, *16*, 1954. https://doi.org/10.3390/en16041954

Academic Editor: Lorand Szabo

Received: 15 December 2022
Revised: 10 February 2023
Accepted: 14 February 2023
Published: 16 February 2023

1. Introduction

Pneumatic motors are widely used in the robotic, automation, and automotive industries. Compared to electric motors, a pneumatic motor has the benefits of large payload-to-weight and payload-to-volume ratios, and high speed and force capabilities [1–6]. By using an air motor to provide rotary actuation instead of electric motors in robotic actuators, they receive high power-to-weight and power-to-size ratios, good compliance, and resistance to environmental hazards [1]. A hybrid pneumatic combustion engine also enhances the fuel economy by recovering wasted energy during engine braking [2,3]. A pneumatic engine is capable of storing energy in the form of compressed air in combustion engines to save 30% fuel consumption in small combustion engines [4,5]. Pneumatic motors are compact and lightweight. A pneumatic motor also has adjustable torque by regulating inlet gas pressure, and there is no overheating problem. Moreover, to avoid electricity usage, pneumatic motors can work under explosive and volatile atmospheres [7].

A significant shift towards renewable energy has been the primary focus of many areas and countries in the last decade. New applications for pneumatic motors such as small-scale expanders have been fit in effective exhaust or cooling systems such as the organic Rankine cycle and Kalina cycle [8,9] because heat-driven power generation process

is exceptionally effective at low-temperature heat conversion. Waste-heat recovery has been a recent implementation and yields more efficient energy conversion that, in turn, decreases harmful pollution emissions on a large scale. A similarly structured machine is also used as an expander in the power generation system of the organic Rankine cycle (ORC) and energy storage system of compressed air energy storage [10], which is a vital component for system performance.

Different types of pneumatic motors (or gas expanders) are available, including the scroll [11], screw [12], piston [13] and vane [14] types. Pneumatic radial piston motor has advantages over the commonly used rotary vane-type motor: higher efficiency, torque, and power output. Bianchi et al. [15,16] used a radial piston expander with three cylinders placed at 120° that shared a crankshaft in their ORC system. The expander and connected generator generated 250–1200 W of electricity with a constant total efficiency of around 40%. Two semiempirical models of a radial piston expander were compared and used for more comprehensive unexplored operational conditions; the results indicated that the lumped parameters model had better accuracy than that of a polynomial fitting model. Han et al. [17] tested a radial piston expander with five cylinders in an ORC system; the results showed the highest isentropic efficiency of 64.8% and the highest mechanical efficiency of 51.0%. Fukuta et al. [18], and Ferrara et al. [19] used a radial piston expander in CO_2 refrigeration systems to conduct work recovery by replacing the throttling valve. The former study achieved mechanical efficiency of 50–60% and overall expander efficiency of about 40%. The measured total efficiency of the used expander in the latter study was 19%, which increased the refrigeration cycle's efficiency by 7.4%.

Although there are several researchs don on modelling of compression and compressors [20], the modelling and simulation of a radial piston motor/expander have rarely been reported. In this study, a commercial pneumatic radial piston motor was modelled and experimentally tested. Volume equation, heat transfer correlation, thermodynamic energy conservation equation, and motion equation were linked to the simulation of the rotation of this motor. One of the crucial parameters of the motor, the overall friction coefficient, was used to simplify the modelling; however, its value was unknown and impossible to obtain through the calculations.

This article aims to model a radial pneumatic piston motor. Previous studies were carefully considered because of the lack of similarities shared between small-scale expanders. The technology for the pneumatic radial piston motor is exceptionally recent. However, using the ORC and Kalina cycle's highest-rated expanders opens up a wide range of resources. Experimental results are fitted into functions to support the accuracy of the simulation. Using the same method as that developed in [21] for scroll expander modelling and simulation, we fed the experimental results into the simulation to determine the value of this coefficient and obtain an accurate simulation that could be used to numerically study the system performance within a broader range of operational conditions, and guide the further design and optimisation of such motors/expanders. This allows for the additional exploration of the geometrical model and its performance. The expander is first geometrically and thermodynamically described, followed by stabilising the whole model and simulation. The experimental results are presented to give further insight into parameters that are tough to test or measure, such as the overall system friction factor, and to validate the simulation.

2. Working Principle

The pneumatic radial piston motor used in this study was supplied by PTM Mechatronics (model no.: PTM3600 VA G3 B1 Ex S) (https://ptm-mechatronics.com/en/products/compressed-air-motors/stainless-steel-motor/), and its photo and interior structure are shown in Figure 1. It has an innovative design of seven pistons in a star pattern moving along an inner curved piston guide. Sustainable efficiency could be achieved with high torque at minimal gas intake, low rotational speed, and reversible rotating direction. It also operates without piston rods or a crankshaft and has a long service life with little

maintenance, in addition to instantaneous stop-and-starts with a high starting torque. In manipulating the inlet gas pressure, each piston cylinder uses a single valve to compress, expand, intake, and discharge the working gas. The motor works without a crankshaft or piston rods, has a 1:2 gear ratio, its rotational speed is between 60 and 600 rpm, with minimal and maximal torques of 1.5 and 16 Nm, respectively. The motor could generate maximal power of about 250 W. The application temperature range of the working gas was from −10 to 80 °C. The operating pressure was in the range of 2–8 bar.

The motor has seven piston cylinders arranged in a star pattern. Each piston is connected to a guide roller at the bottom, allowing for the piston to glide along the curved inner surface of the housing. High-pressure gas enters the motor through the fixed piston control shaft via the floating piston control ring to individual pistons. The motor has four cross-arranged inlets and four cross-arranged outlets, as shown in Figure 1. When it rotates, the working gas in the piston cylinders changes between charge and discharge.

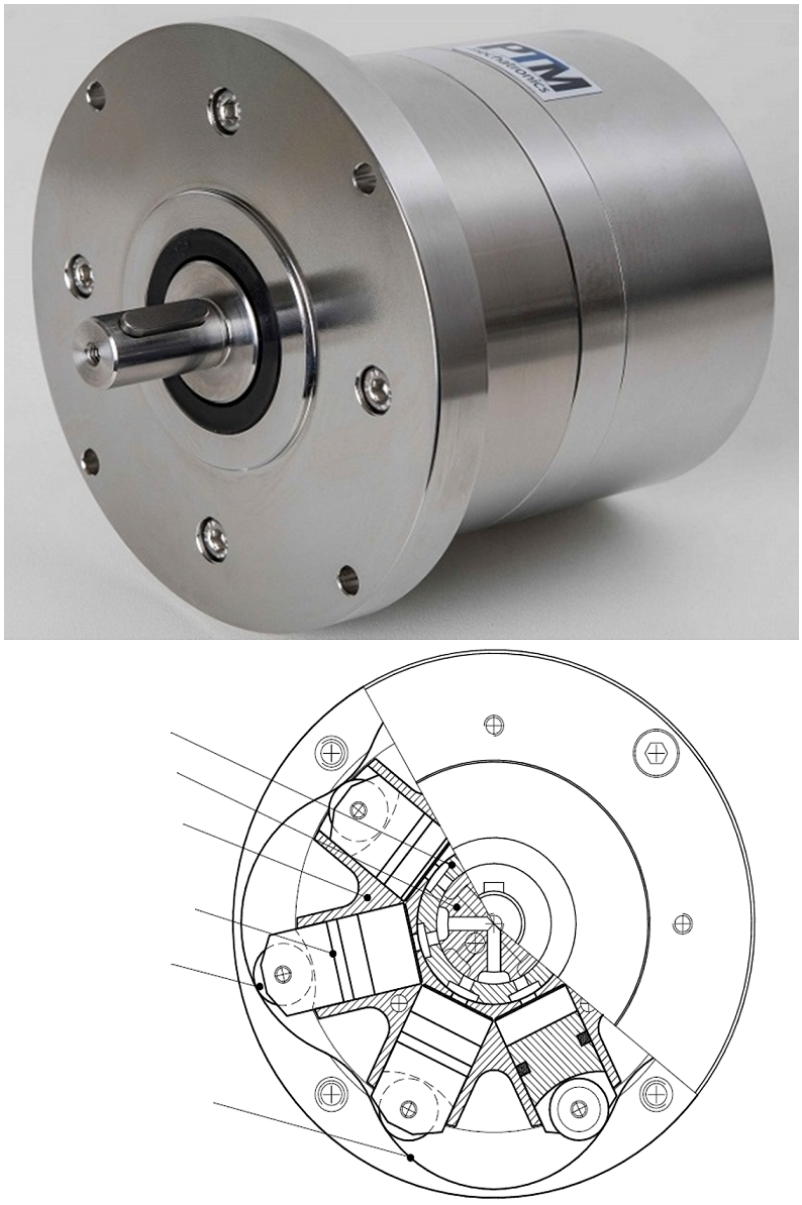

Figure 1. Photo and interior structure of the studied pneumatic motor.

During rotation, three of the seven piston cylinders are primarily responsible for generating a positive torque for rotation. The pressure difference between the working gas and back (ambient) pressure generates the force exerted at the contact point of the roller

and guide curve along the direction from the motor centre to the roller centre (the normal direction of the piston), as shown in Figure 2. This force can be divided into two component forces: one drives rotation, while the other presses perpendicularly on the glide surface, which generates friction.

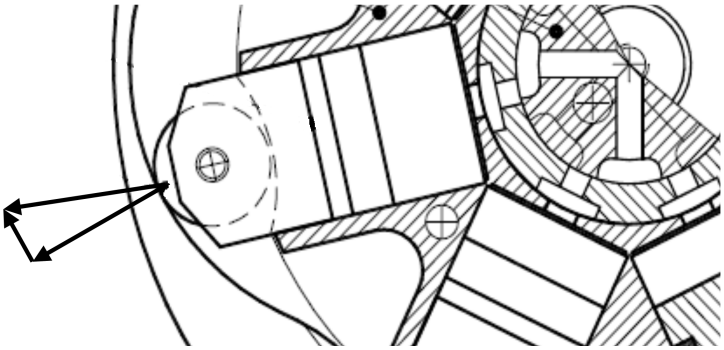

Figure 2. Driving force of the motor rotation.

2.1. Geometric Description of the Expander

Before modelling, the primary issue is to geometrically understand the piston motor. The detailed geometric information was obtained by analysing the cross-section, drawn as given in Figure 1. The motor manufacturer gave the housing diameter ($2R_1$) and the distance from the motor centre to the upper surface of the piston cylinder (R_4). On the basis of the available R1, other dimensional parameters were proportionally calculated, as illustrated in Figure 3. The calculated values are presented in Table 1. The method was reliable, as there was only a minor error when comparing the calculated R4 and the value provided by the motor manufacturer.

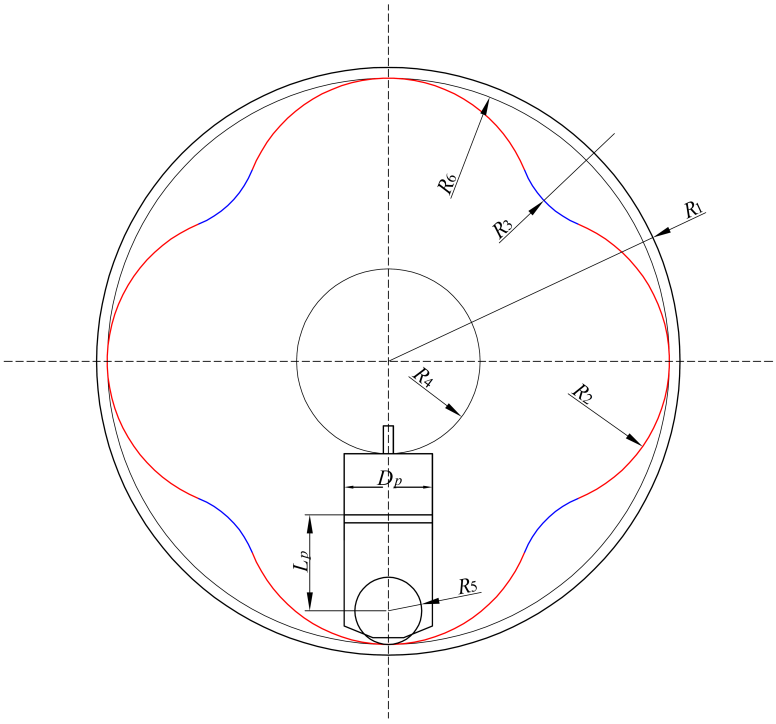

Figure 3. Key dimensional parameters.

Table 1. Geometrical parameter values of the expander motor.

Parameter	From Manufacturer Manual (mm)	Calculated (mm)
Housing diameter ($2R_1$)	159	-
Concave circle diameter ($2R_2$)	-	80.23
Convex circle diameter ($2R_3$)	-	52.84
Motor centre to cylinder upper surface (R_4)	25	24.95
Roller diameter ($2R_5$)	-	18.20
Concave circle to motor centre (R_6)	-	76.61
Cylinder diameter (D_p)	-	24.03
Roller centre to piston upper surface (L_p)	-	35.07

The unique piston glide curve leads to complicated geometric calculations for the piston cylinder, which encompasses cycle segments with two different diameters, one concave with a larger radius R_2, and the other convex with a smaller radius R_3. Locating the centres of these circular segments and knowing their diameters are essential for understanding the rotation of pistons. Knowing the positions of the joint points of circle segments is also crucial. This study set the rotational angle at 0° when the piston cylinder was at the position shown in Figure 3, and the rotation was clockwise. A critical rotational angle, α, is defined as the angle when the roller transits from gliding on the concave circle to the convex circle, as shown in Figure 4a. The following equations were used to calculate α:

$$L_1 = R_6 - R_2 \tag{1}$$

$$\beta = arcsin(\frac{\frac{\sqrt{2}}{2} L_1}{R_2 + R_3}) \tag{2}$$

$$\gamma = \frac{3}{4}\pi - \beta \tag{3}$$

$$L_3 = \sqrt{{L_1}^2 + (R_2 - R_5)^2 - 2(R_2 - R_5)\, L_1\, cos\gamma} \tag{4}$$

$$\alpha = arcsin(\frac{(R_2 - R_5)sin\gamma}{L_3}) \tag{5}$$

When rotational angle θ satisfies $i\pi/2 - \alpha \leq \theta \leq i\pi/2 + \alpha$, where (i = 0, 1, 2, 3), the piston roller glides along the concave circle curve as shown in Figure 4b; otherwise, the roller glides along the convex circle curve as shown in Figure 4c. The length from the motor centre to the piston roller centre L4 in Figure 4 is the critical parameter to calculate the interior volume of the piston cylinder. Equations (6) and (7) were used to calculate L4 in Figure 4b, and Equations (8) to (10) were used to calculate L_4 in Figure 4c.

$$L_5 = R_2 - R_5 \tag{6}$$

$$L_4 = L_1 cos\theta + \sqrt{{L_5}^2 - (L_1 sin\theta)^2} \tag{7}$$

$$L_2 = \frac{\sqrt{2}}{2} L_1 + \sqrt{(R_2 + R_3)^2 - \frac{{L_1}^2}{2}} \tag{8}$$

$$L_6 = R_3 + R_5 \tag{9}$$

$$L_4 = L_2 cos(\frac{\pi}{4} - \theta) - \sqrt{{L_6}^2 - (L_2 sin(\frac{\pi}{4} - \theta))^2} \tag{10}$$

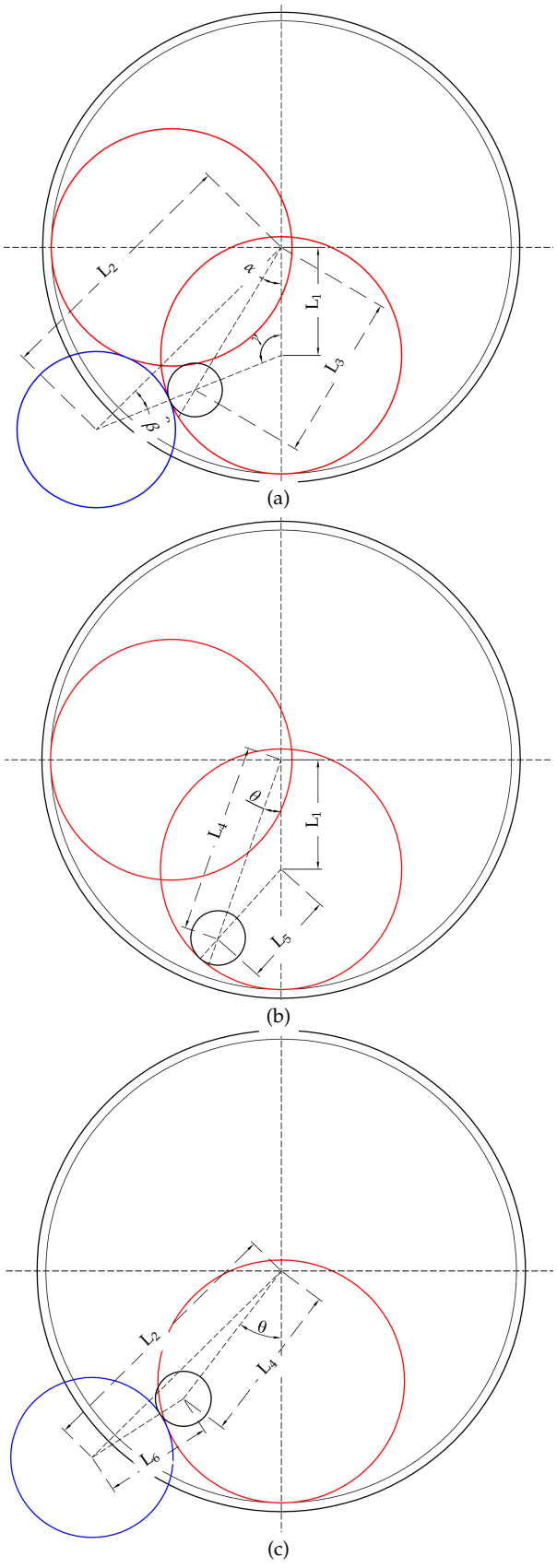

Figure 4. Determination of cylinder volumes. (**a**) Critical rotational angle; (**b**) contact point of roller with concave circle; (**c**) contact point of roller with convex circle.

Volumetric change in the piston cylinder could be calculated from 0 to $\pi/4$, mirrored from $\pi/4$ to $\pi/2$, and the same variation can be repeated to 2π at every $\pi/4$. Once L_4 is known, the interior volume of a single piston cylinder can be determined by calculating the following equation:

$$V = \frac{\pi(L_4 - R_4 - L_p){D_p}^2}{4} \tag{11}$$

The result is presented in Figure 5; one piston experienced 4 times the gas charge and discharge in each motor rotation.

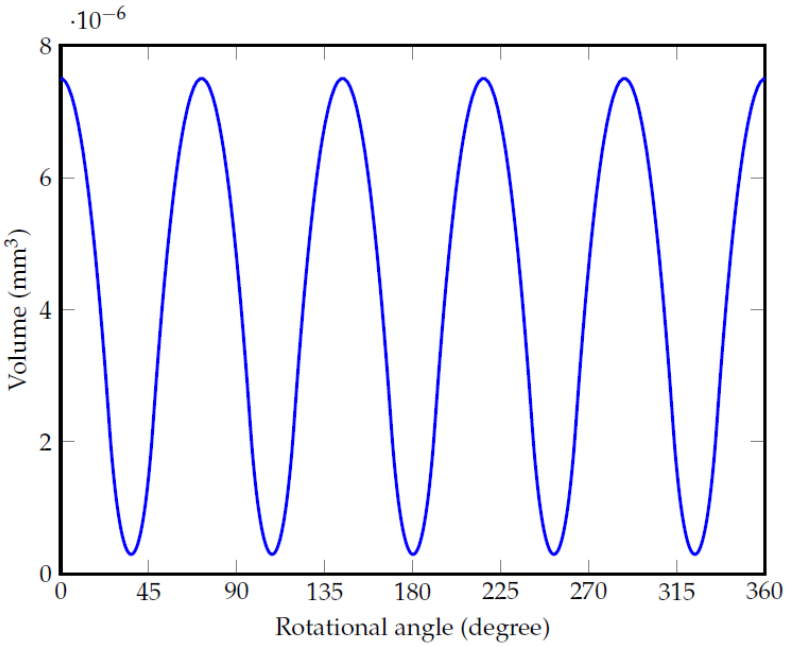

Figure 5. Single cylinder volume vs. rotational angle.

2.2. Thermodynamic Model

The process inside the pneumatic motor follows the first thermodynamic law in an open control volume, as given in the following equation.

$$\frac{d(mu)}{dt} = \dot{Q} - P\frac{dV}{dt} + \dot{m}_{in}h_{in} - \dot{m}_{out}h \tag{12}$$

where m is the mass of the gas inside the control volume, u is the specific internal energy, $\dot{Q}$ is the heat transferred from the surroundings to the gas inside the cylinder, P is the gas pressure, V is the gas volume, t is the time, $\dot{m}_{in}$ is the inlet gas mass flow rate, h_{in} is the inlet gas enthalpy, $\dot{m}_{out}$ is the outlet gas mass flow rate, and h is the gas enthalpy. The equation can be reorganised by replacing internal energy with h-Pv (v is the specific volume) as given in the following equations:

$$\frac{d(mh - PV)}{dt} = \dot{Q} - P\frac{dV}{dt} + \dot{m}_{in}h_{in} - \dot{m}_{out}h \tag{13}$$

$$\frac{d(mh)}{dt} = \dot{Q} + V\frac{dP}{dt} + \dot{m}_{in}h_{in} - \dot{m}_{out}h \tag{14}$$

$$m\frac{d(h)}{dt} + h\frac{d(m)}{dt} = \dot{Q} + V\frac{dP}{dt} + \dot{m}_{in}h_{in} - \dot{m}_{out}h \tag{15}$$

For the gas suction process, the following equation is obtained considering that no gas was exiting:

$$m\frac{d(h)}{dt} + h\dot{m}_{in} = \dot{Q} + V\frac{dP}{dt} + \dot{m}_{in}h_{in} \quad (16)$$

During compression and expansion, there is no gas leakage between cylinder and the atmosphere, and no gas entering and exiting; the following equation is obtained:

$$m\frac{d(h)}{dt} = \dot{Q} + V\frac{dP}{dt} \quad (17)$$

For the gas discharge process, considering that no gas was entering, and the enthalpy of exiting gas was the same as the gas enthalpy within the cylinder, the same equation as Equation (17) was obtained. The heat transfer between the gas inside the piston cylinder and the ambient air is unique because the piston undergoes four different progressions. The heat transfer rate can be calculated with the following equation:

$$\dot{Q} = \frac{T_a - T_g}{\frac{1}{A_c H_a} + \frac{\delta_c}{k_c} + \frac{1}{A_c H_g}} \quad (18)$$

where h is the heat transfer coefficient, k is thermal conductivity, δ is thickness, and subscripts a, c, and g represent the ambient air, cylinder wall, and working gas, respectively. A_c is the contact surface area of the working gas with the cylinder, which varies as the piston moves inside the cylinder. H_a is the heat transfer coefficient of natural air convection. H_g can be determined by using the following empirical correlation proposed by Tuhovcak et al. [22]:

$$Nu = aRe^b Pr^c \quad (19)$$

where Nu is the Nusselt number, Re is the Reynolds number, Pr is the Prandtl number, and a, b, and c are constants. Due to the movement of the piston, the Reynolds number and constants are different for suction, compression, discharge, and expansion processes, which are detailed in Table 2. The used U_p is the piston speed, and U_g is the effective gas velocity caused by suction or discharge, which the following equation can determine:

$$U_g = \frac{|\dot{m}|}{\rho A_c} \quad (20)$$

Table 2. Reynolds number and constant values in Equation (20) [22]. (ρ is fluid density (kg/m^3), V_p is the average flow velocity (m/s), D is the hydraulic diameter (m), μ is the dynamic viscosity coefficient (kg/ms).

Process	Reynolds Number	a	b	c
Compression	$\rho D V_p/\mu$	0.08	0.8	0.6
Discharge	$(\rho D V_p + V_p^{0.8} V_c^{0.2})/\mu$	0.08	0.8	0.6
Expansion	$\rho D V_p/\mu$	0.12	0.8	0.6
Suction	$(\rho D V_p + V_p^{-0.4} V_c^{1.4})/\mu$	0.08	0.9	0.6

2.3. Dynamic Motion

The rotational speed of the motor relies on the pressure difference between supplied gas and ambient air. The following motion equation determines the rotational speed:

$$\Sigma J\frac{d\omega}{dt} = \Sigma Tu_t - Tu_{fr} \quad (21)$$

where J is the inertia of the rotational parts, ω is the rotational angle speed (rad/s), and Tu_t and Tu_{fr} are the summaries of the driving torque generated by each piston and the

overall friction torque of the motor, respectively. Torques can be calculated on the basis of the forces exerted on the contact points of the piton roller and glide curve, as shown in Figure 6. The working gas was sealed in the cylinder, but within the shell, there was still ambient air; therefore, the pressure difference between the internal working gas and the ambient air generates the force driving the rotation. The force had a direction from the motor centre to the roller centre, which can be determined with the following equation:

$$F_i = A_{\mathrm{p}}(P_{\mathrm{i}} - P_{\mathrm{a}}) \tag{22}$$

where A_{P} is the cross-sectional area of the piston, i indicates a different piston, and a indicates the ambience.

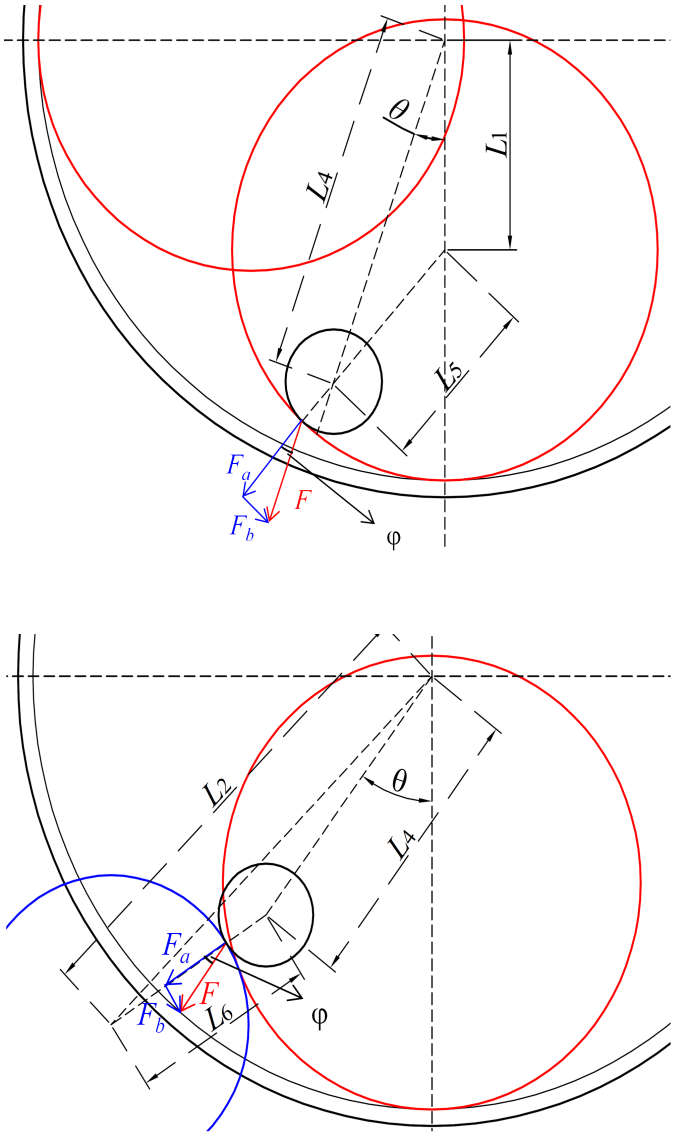

Figure 6. Forces and their components.

The force can be divided into two component forces: F_{a} follows the direction from the glide curve centre to the roller centre, and F_{b} follows the corresponding perpendicular direction, as shown in Figure 6. F_{a} causes friction that holds back the rotation. The driving force for the rotation, F_{b}, can have both positive and negative effects on the rotational subjects on the rotational angle. For example, rotating in the clockwise direction, F_{b} in Figure 6 had a negative effect, and the gas inside the cylinder underwent compression.

During expansion, F_b flips its direction and positively affects the rotation. Simultaneously, the motor had seven rotating pistons, and the total effect of F_b positively drove the motor. Angle ϕ between the directions of F and F_a, as shown in Figure 6, could be calculated with the following equations:

$$\phi = arcsin(\frac{L_1 sin\theta}{L_5}) \tag{23}$$

$$\phi = arcsin(\frac{L_2 sin(\frac{\pi}{4} - \theta)}{R_3 + R_5}) \tag{24}$$

where Equation (23) is valid when the roller glides on a concave cycle, and Equation (24) is valid when the roller glides on the convex cycle. ϕ should be given a negative sign when $0 < \theta \leq \pi/4$ because both F_a and F_b have adverse effects on rotation; then, ϕ is positive when $\pi/4 < \theta \leq \pi/2$ and repeats every $\pi/2$.

Then, the motion equation can be rewritten as follows:

$$\Sigma J \frac{d\omega}{dt} = \Sigma(F_i sin\phi - f_r F_i cos\phi) r_i - \omega f_{overall} \tag{25}$$

where f_r is the roller friction factor, $f_{overall}$ is the overall system friction coefficient, and r_i is the distance from the tough point of the roller and the glide curve to the motor centre. $f_{overall}$ is usually unknown and difficult to estimate. In the current study, experimental results were introduced into the simulation to fit the equation and determine the value of $f_{overall}$.

2.4. Modelling Algorithm

There were seven cylinders in the studied motor. However, only a single piston was simulated because of the consistency of the others. We hypothesised the following to reasonably simplify the motor simulation.

- The gas leakage through the reed valve was negligible.
- The pressure drop through the inlet/outlet was predefined at a fixed value (1 kPa); therefore, the gas pressure inside the motor had no change during suction and discharge stages under constant supplied gas pressure and back pressure.

To support the assumption of negligible leakage (Figure 7), there was the reverse relationship between rotational speed and the amount of leakage. Leakage for expanders at higher rotational speeds converges to zero; as a result, the efficiency of the motor is better at higher rotational speed [23].

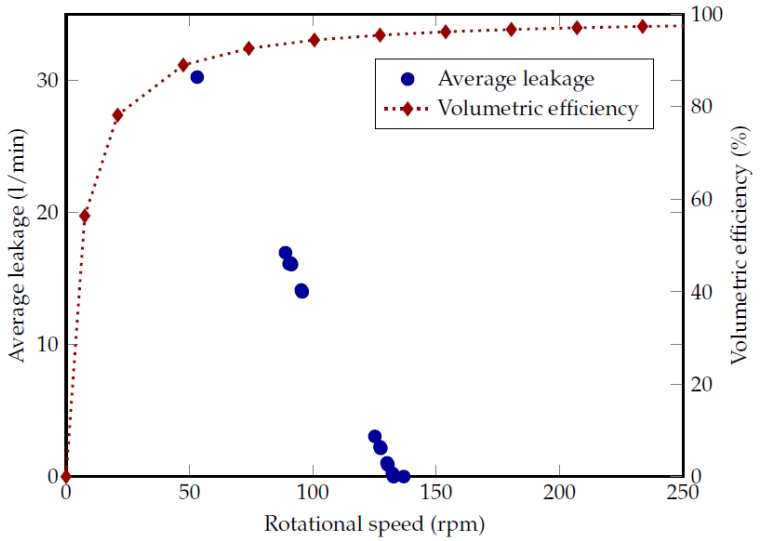

Figure 7. The effect of rotational speed on average leakage and volumetric efficiency [23].

Air was used as the working gas for this simulation and experimental validation. The thermophysical properties of air, including specific heat, density, enthalpy, thermal conductivity, and viscosity, were correlated as the function of temperature, pressure, and humidity [24,25]. The following procedure was used for the motor simulation.

- The motion equation was solved on the basis of the previous gas state inside the cylinder and the present rotational speed, and the rotational angle was obtained.
- The present rotational angle was used to determine the present cylinder volume.
- The present rotational angle was used to determine the stage of the process, i.e., compression, discharge, expansion, or suction.
- The thermodynamic equation and heat transfer correlation were used to calculate the present gas pressure, temperature, and other thermodynamic properties on the basis of the determined stage of the process and the gas volume.
- The mass flow rates at the suction and discharge stages were determined on the basis of the invariable gas pressure at these two stages.
- The calculation iterates until it reaches steady-state operation or the predefined operational time.

The flowchart of the model is illustrated in Figure 8.

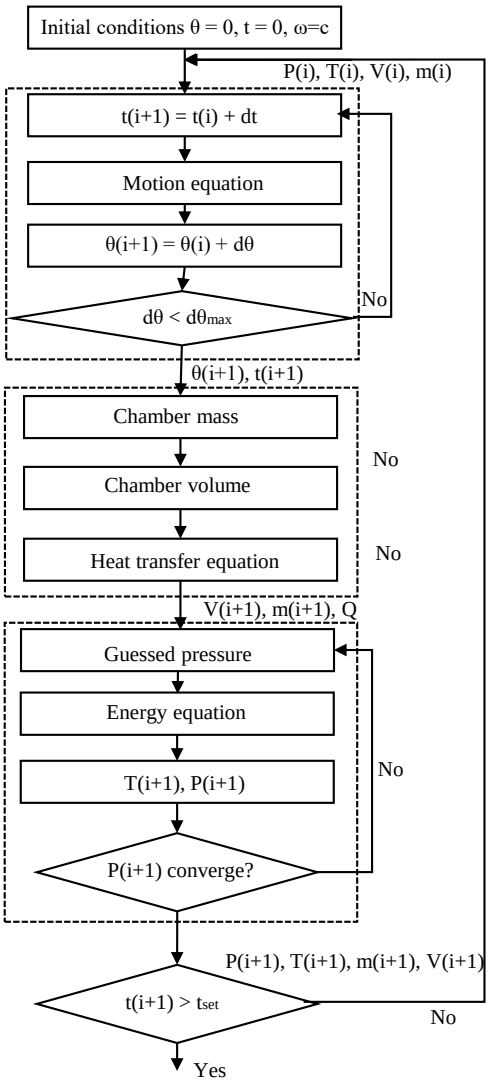

Figure 8. Flowchart for the model algorithm.

3. Simulation Model

The mathematical model incorporated several parameters of the given expander. The validation of the simulation was measured using the test results. Choosing a correct time step is essential to obtain precise results, and it must be understood when evaluating the simulation time incrementation. First, i < 5000 increments were used,and the rotational speed levelled out consistently. The change in time was set at dt = 0.000075 s, and i < 5000 steps simulated only 0.375 s. After ignoring the first 4500 time steps, the rotational speed flattened out and accurately gave the average speed in RPM. Results were compared, increasing from 5000 to 10,000, which ranged from 0.375 to 0.75 s. Taking into consideration the computational time, 9000 steps were chosen to yield the most promising results.

One simulated dynamic rotation process is exemplified in Figure 9 with inlet air pressure at 2.0 bar (absolute pressure). Once the motor had been connected to the compressed air, the rotation of the motor quickly reached a steady state; in this specific case (2 bar), the rotational speed reached an almost constant value of around 395 rpm.

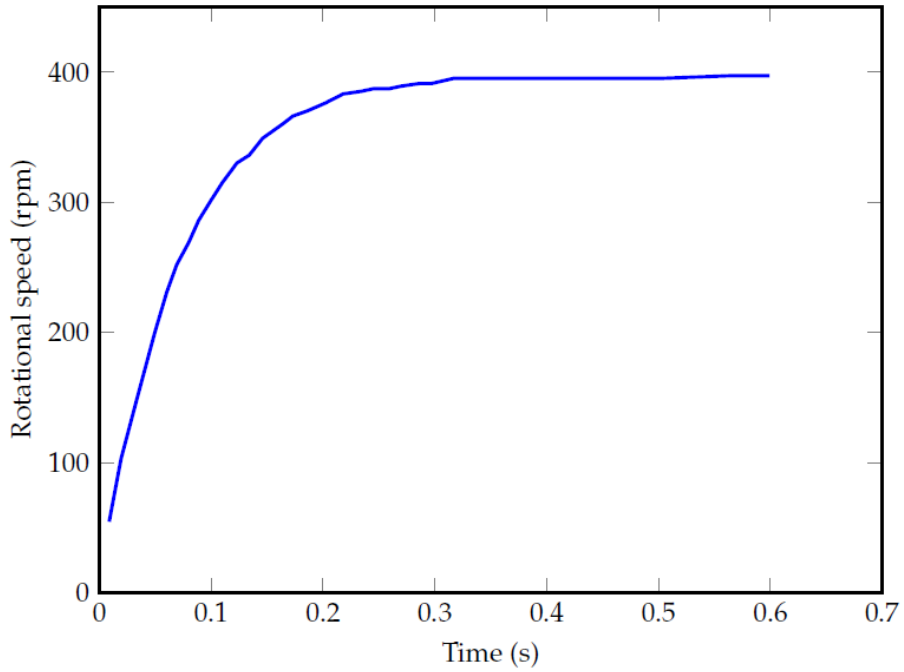

Figure 9. Example of rotational speed vs. time, P_{in} = 2.0 bar (absolute value).

4. Experimental Apparatus

The motor was tested without connection to any load. The experimental setup and its schematic diagram are given in Figure 10. Compressed air at 6 bar (gauge pressure) was used as supplied gas for testing. A regulator was used to regulate the pressure of gas entering the motor. A rotameter (10–100 L/min) was used to measure the volumetric flow rate of the air, and a pressure gauge (0–6 bar) was used to measure the air pressure. A tachometer (Voltcraft DT-10L) was used to measure the rotational speed of the motor shaft. The tests were conducted with relatively low air pressure due to the lack of a load in order to restrict the rotational speed to lower than 600 rpm (the maximal speed provided by the manufacturer). The test results with varying inlet air pressure and shaft rotational speed are presented in Table 3.

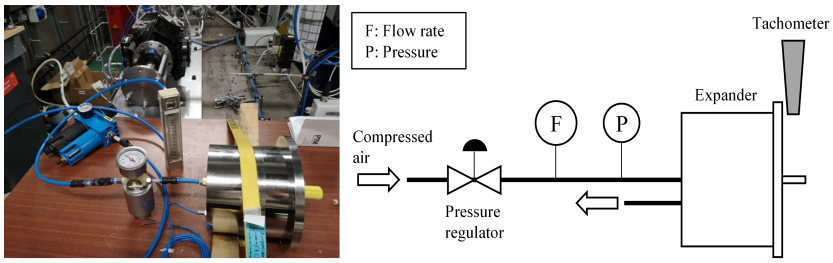

Figure 10. Experimental setup and schematic diagram of the expander motor.

Table 3. Experimental test apparatus outcomes.

Absolute Inlet Air Pressure (bar)	Inlet Volumetric Flow Rate (L/min)	Shaft Rotational Speed (rpm)
1.60	44.0	232.3
1.70	51.0	272.9
1.80	54.0	313.8
1.83	58.0	326.1
1.85	62.0	333.6
1.95	67.0	374.5
2.00	55.0	394.8

5. Results and Discussion

In order to understand if the model is working properly, in the first step, the model needed to be validated. Therefore, further analyses were carried out to analyse the expander efficiency and the sensitivity analysis of the effective parameters on the performance of the expander.

The overall motor friction coefficient ($f_{overall}$) in Equation (25) was carefully determined by comparing the simulated and experimental results (inlet air pressure vs. rotational speed) while adjusting the input value of $f_{overall}$ in the simulation. The value of 0.0625 Nm was obtained, which led to satisfactory agreement between the experimental and simulated values of the rotational speed at different inlet air pressure levels, as shown in Figure 11.

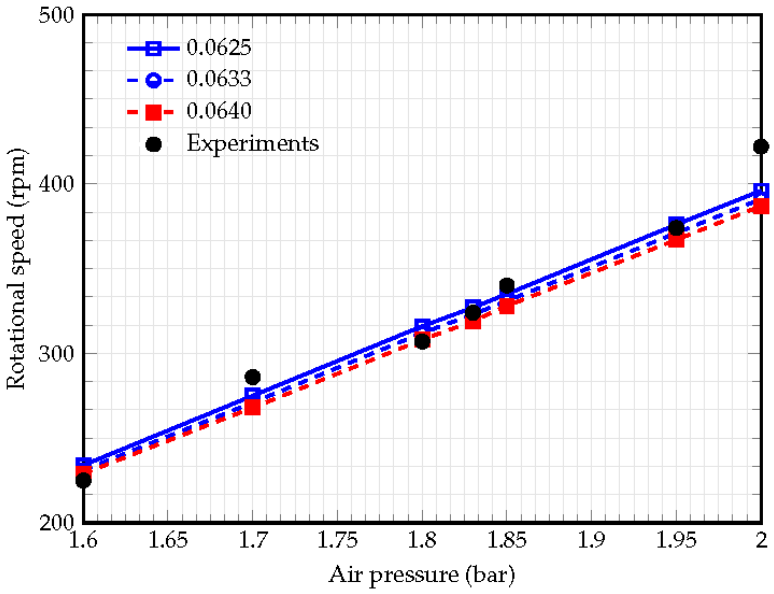

Figure 11. Comparison of experimental and simulated rotational speed vs. inlet air pressure with $f_{overall}$ of 0.0625, 0.0633, and 0.0640 Nm.

Figure 11 shows the inlet pressure, and experimental and simulated results varying the friction factor. In Figure 11, inlet pressure starting at 1.6–2 bar was investigated. The overall system friction values were also estimated at the given value. The resulting rotational

speed was averaged over 5000–9000 steps to reveal a result in rpm. Eventually, the friction factor of 0.064 started to align with the test results.

Under close observation, the values were in a similar range, varying by 3 to 4 rpm with a change of 0.007 to the friction factor. Values above 0.064 were dismissed because of the low outputs. With the use of the experimental results, the unknown friction factor was easily detected. Throughout the literature, many CFD models follow the same method. The value is tough to measure and involves complex mathematical analysis. The overall factor involves several moving components, and as a system, changes between each process fluctuate with unknown parameters. Due to friction, energy dissipation and internal flow losses are experienced. The expander is an open-drive system without a generator in both experimental tests and simulations. Studies were confronted with constant mechanical loss [26] with the absence of a generator.

If a system were connected to an electrical generator, the expander loss would be proportional to the generator's energy loss.

Comparing the simulated model to known results lies within the system's desired performance. Below are the experimental test results with estimated overall frictional coefficients of 0.064, 0.0633, and 0.0625 Nm from a given inlet pressure.

The experimental results skewed more at 1.7 and 2 bar than at 12 rpm. However, considering more than 71% of the remaining data points shows a tightly correlated relationship, which suggests the successful validation of the simulation. The overall friction factor of 0.0625 Nm was the most promising in terms of accuracy. Likewise, the value was 0.064 because numerous other inputs have failed to show capable results. The rotational speed was averaged over the time range from 0.0375 to 0.675 s and was stable. As the rotational speed increased, it began to stabilise because friction is proportional to the drag torque, and at a specific point, friction becomes too large. The drag slows down the driving force and rotational inertia.

The model allows for a new design attempt too, primarily investigating the diameter inlet point, the diameter of the cylinder, and piston length in terms of overall performance. Changing the design parameters while using the same inlet pressure and outputting a higher rotational speed achieved better performance. On the basis of the simulation, the diameter of the piston was adjusted from the design value of 24.02517 mm. In Figure 12, the results of the piston diameter are expressed. The optimisation of the simulation began by increasing the diameter of the piston. The highest rotational speeds were achieved using a diameter of 25.8 mm. The original design parameter is shown as the bottom line in Figure 12.

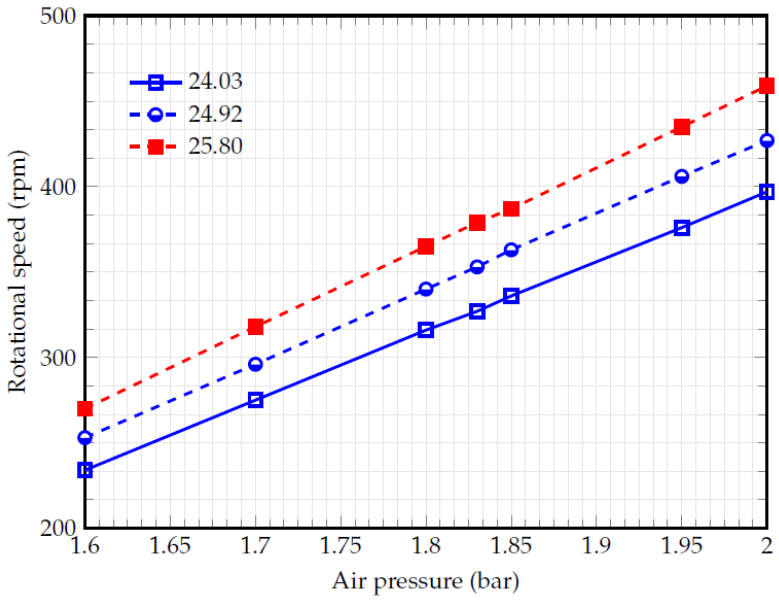

Figure 12. Rotational speed vs. inlet pressure by changing piston cylinder's diameter.

According to Figure 13, the mass of the fluid inside the chamber had a direct relationship with the volume of the chamber (see Figure 5). The mass remained constant at the beginning of the expansion and compression stages; however, the exhaust/intake valve had been open before expansion/compression was completed. On the other hand, pressure remains constant during the intake and exhaust stages (the exhaust pressure level is lower than the intake). The sharp peak of the pressure profile is due to the valve motion and the sudden presence of the high-pressure gas in the chamber. In an expander, a pressurised fluid's energy is transformed into mechanical energy by increasing its volume and decreasing its pressure. According to Figure 14, the peak of outlet mass flow rate of the expander (sum of all 7 cylinders) was 0.02 kg/s and 5 times higher than the inlet mass flow rate. However, the minimal value of the mass flow rate in the outlet was half of the value in the inlet.

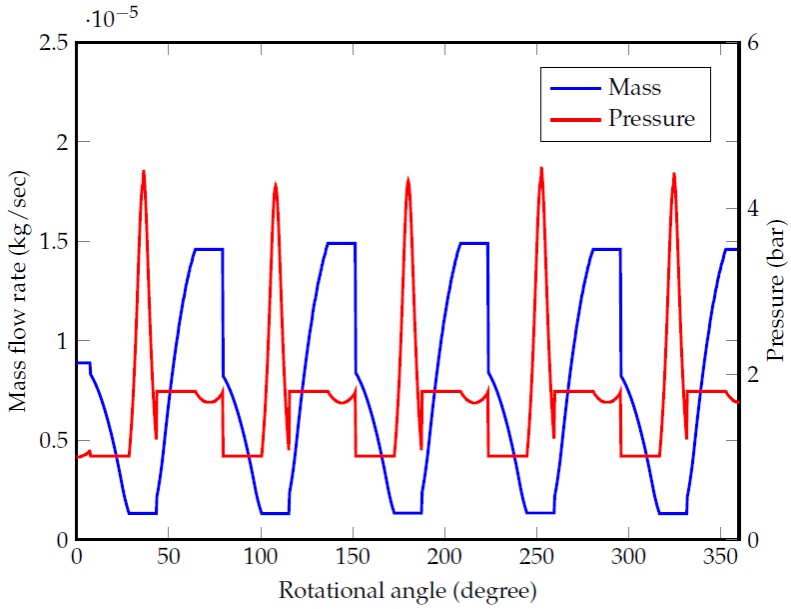

Figure 13. Single cylinder mass and pressure behaviour as a function of the rotational angle.

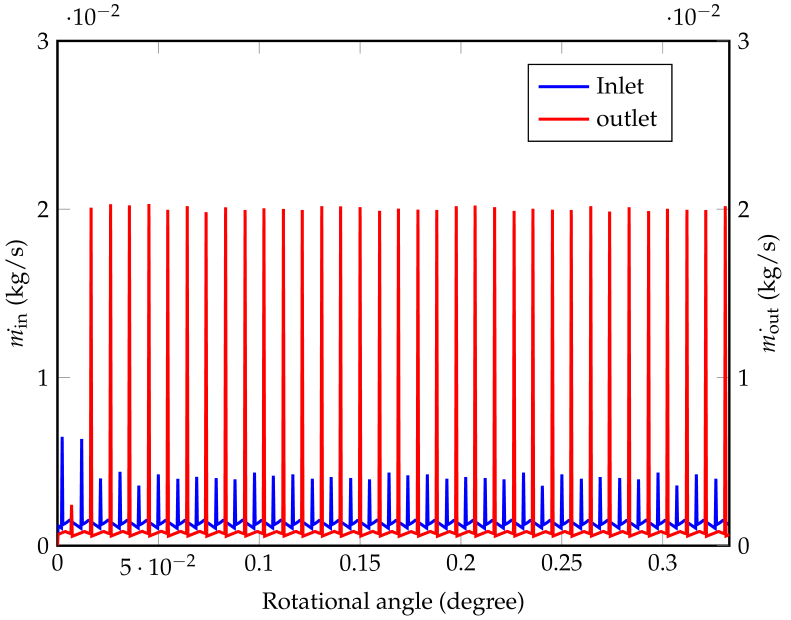

Figure 14. Single cylinder mass and pressure behaviour as a function of the rotational angle.

6. Conclusions

This study presented the detailed models and simulation processes of a pneumatic radial piston motor (expander). One of the crucial parameters, the overall friction coefficient of the motor f_{overall}, was used to simplify the modelling. However, its value was unknown. The value was determined by introducing the experimental test results to the simulation, of which the value was 0.0625 Nm. Such a method is generic and does not need cumbersome relation formulation. A new build for the expander could be examined by changing the design parameters. The same inlet pressure was used, and greater rotational speeds were achieved by increasing the cylinder's diameter to 25.8 mm. Accurate values of the f_{overall} of each motor or motor–load system should be determined by feeding several groups of experimental test results into a simulation. Then, the simulation with the correct overall friction coefficient can be used to guide the design and optimisation of the motor, and to predict the motor performance in a broader range of operational conditions. The model can also estimate other design parameters of expanders; in this paper, a design diameter of 25.8 mm was suggested for the highest rotational speed.

Author Contributions: Conceptualisation, K.G., Z.M., and A.N.; methodology, K.G., A.N., and H.B.; modelling, K.G. and Z.M.; validation, A.N.; investigation, A.N.; writing—original draft, K.G., A.N., and Z.M.; supervision, Z.M., H.B., and T.R. All authors have read and agreed to the published version of the manuscript.

Funding: the authors gratefully acknowledge the support from the Solar S&HP project (code EP/T023090/1), and funding from the Engineering and Physical Science Research Council (EPSRC), UK.

Data Availability Statement: Data are available on request due to privacy or ethical restrictions. The data presented in this study are available on request from the corresponding author.

Conflicts of Interest: The authors declare no conflict of interests.

Abbreviations

The following abbreviations are used in this manuscript:

Greek symbuls	
$\alpha, \beta, \gamma, \theta, \psi$	Angel (rad)
δ	Thickness (m)
ρ	Three letter acronym
μ	Viscosity (Pas)
ω	Angular velocity (rad/s)
μ	Density (kg/m$_3$)
Subscript	
a	Ambient
c	Cylinder
fr	Friction
g	Gas
P	Piston
t	Torque
Symbols	
$\dot{m}$	Mass flow rate (kg/s)
$\dot{Q}$	Heat transfer rate (W)
A	Area (m^2)
D	Diameter (m)
F	Force (N)
f_{overall}	Overal dynamic friction coefficient (Nms)

f_r	Roller friction factor (−)
h	Enthalpy (J/kg)
m	Mass (kg)
P	Pressure (Pa)
Pr	Prandtl number (−)
R	Radius (m)
r	Distance (m)
Re	Reynolds number (−)
T	Temperature (K)
t	Time (s)
Tu	Torque (Nm)
U	Velocity (m/s)
u	nternal energy (J/kg)
V	Volume (m^3)
H	Heat transfer coefficient (W/m^2K)
J	Moment of inertia (kgm^2)
k	Thermal conductivity (W/mK)
L	Lenght (m)
Nu	Nusselt number (−)

References

1. Pandian, S.R.; Takemura, F.; Hayakawa, Y.; Kawamura, S. Control performance of an air motor-can air motors replace electric motors? In Proceedings of the 1999 IEEE International Conference on Robotics and Automation (Cat. No. 99CH36288C), Detroit, MI, USA, 10–15 May 1999; IEEE: Piscataway, NJ, USA; Volume 1, pp. 518–524.
2. Fang, Y.; Lu, Y.; Yu, X.; Su, L.; Fan, Z.; Huang, R.; Roskilly, A.P. Study of a hybrid pneumatic-combustion engine under steady-state and transient conditions for transport application. *Int. J. Engine Res.* **2021**, *22*, 528–539. [CrossRef]
3. Basbous, T.; Younes, R.; Ilinca, A.; Perron, J. Required time response of a variable valve actuator equiping a hybrid pneumatic–combustion engine. *Int. J. Engine Res.* **2012**, *13*, 514–528. [CrossRef]
4. Higelin, P.; Vasile, I.; Charlet, A.; Chamaillard, Y. Parametric optimization of a new hybrid pneumatic-combustion engine concept. *Int. J. Engine Res.* **2004**, *5*, 205–217. [CrossRef]
5. Basbous, T.; Younes, R.; Ilinca, A.; Perron, J. Fuel consumption evaluation of an optimized new hybrid pneumatic–combustion vehicle engine on several driving cycles. *Int. J. Engine Res.* **2012**, *13*, 253–273. [CrossRef]
6. Borelli, D.; Devia, F.; Cascio, E.L.; Schenone, C. Energy recovery from natural gas pressure reduction stations: Integration with low temperature heat sources. *Energy Convers. Manag.* **2018**, *159*, 274–283. [CrossRef]
7. Naranjo, J.; Kussul, E.; Ascanio, G. A new pneumatic vanes motor. *Mechatronics* **2010**, *20*, 424–427. [CrossRef]
8. Naveiro, M.; Romero Gómez, M.; Arias-Fernández, I.; Baaliña Insua, Á. Thermodynamic and Economic Analyses of Zero-Emission Open Loop Offshore Regasification Systems Integrating ORC with Zeotropic Mixtures and LNG Open Power Cycle. *Energies* **2022**, *15*, 8622. [CrossRef]
9. Song, P.; Sun, J.; Wang, S.; Wang, X. Multipoint Design Optimization of a Radial-Outflow Turbine for Kalina Cycle System Considering Flexible Operating Conditions and Variable Ammonia-Water Mass Fraction. *Energies* **2022**, *15*, 8748. [CrossRef]
10. Bao, J.; Zhao, L. A review of working fluid and expander selections for organic Rankine cycle. *Renew. Sustain. Energy Rev.* **2013**, *24*, 325–342. [CrossRef]
11. Song, P.; Wei, M.; Shi, L.; Danish, S.N.; Ma, C. A review of scroll expanders for organic Rankine cycle systems. *Appl. Therm. Eng.* **2015**, *75*, 54–64. [CrossRef]
12. He, W.; Wu, Y.; Peng, Y.; Zhang, Y.; Ma, C.; Ma, G. Influence of intake pressure on the performance of single screw expander working with compressed air. *Appl. Therm. Eng.* **2013**, *51*, 662–669. [CrossRef]
13. Zhang, X.; Xu, Y.; Zhou, X.; Zhang, Y.; Li, W.; Zuo, Z.; Guo, H.; Huang, Y.; Chen, H. A near-isothermal expander for isothermal compressed air energy storage system. *Appl. Energy* **2018**, *225*, 955–964. [CrossRef]
14. Chen, S.Y.; Hung, Y.H.; Gong, S.S. Speed control of vane-type air motor servo system using proportional-integral-derivative-based fuzzy neural network. *Int. J. Fuzzy Syst.* **2016**, *18*, 1065–1079. [CrossRef]
15. Bianchi, M.; Branchini, L.; De Pascale, A.; Melino, F.; Ottaviano, S.; Peretto, A.; Torricelli, N. Application and comparison of semi-empirical models for performance prediction of a kW-size reciprocating piston expander. *Appl. Energy* **2019**, *249*, 143–156. [CrossRef]
16. Bianchi, M.; Branchini, L.; Casari, N.; De Pascale, A.; Melino, F.; Ottaviano, S.; Pinelli, M.; Spina, P.; Suman, A. Experimental analysis of a micro-ORC driven by piston expander for low-grade heat recovery. *Appl. Therm. Eng.* **2019**, *148*, 1278–1291. [CrossRef]
17. Han, Y.; Zhang, Y.; Zuo, T.; Chen, R.; Xu, Y. Experimental study and energy loss analysis of an R245fa organic Rankine cycle prototype system with a radial piston expander. *Appl. Therm. Eng.* **2020**, *169*, 114939. [CrossRef]

18. Fukuta, M.; Anzai, F.; Motozawa, M.; Terawaki, H.; Yanagisawa, T. Performance of radial piston type reciprocating expander for CO2 refrigeration cycle. *Int. J. Refrig.* **2014**, *42*, 48–56. [CrossRef]
19. Ferrara, G.; Ferrari, L.; Fiaschi, D.; Galoppi, G.; Karellas, S.; Secchi, R.; Tempesti, D. Energy recovery by means of a radial piston expander in a CO2 refrigeration system. *Int. J. Refrig.* **2016**, *72*, 147–155. [CrossRef]
20. Najjaran, A.; Meibodi, S.; Ma, Z.; Bao, H.; Roskilly, T. Experimentally Validated Modelling of an Oscillating Diaphragm Compressor for Chemisorption Energy Technology Applications. *Energies* **2023**, *16*, 489. [CrossRef]
21. Ma, Z.; Bao, H.; Roskilly, A.P. Dynamic modelling and experimental validation of scroll expander for small scale power generation system. *Appl. Energy* **2017**, *186*, 262–281. [CrossRef]
22. Tuhovcak, J.; Hejčík, J.; Jícha, M. Modelling fluid flow in a reciprocating compressor. In Proceedings of the EFM14 Experimental Fluid Mechanics 2014, EPJ Web of Conferences, Cesky Krumlov, Czech Republic, 18–21 November 2014; Volume 1, pp. 581–586.
23. Rundo, M.; Giavarini, F. Analysis and Simulation of a Radial Piston Hydraulic Motor. Ph.D. Thesis, Politecnico di Torino, Turin, Italy, 2022.
24. Picard, A.; Davis, R.; Gläser, M.; Fujii, K. Revised formula for the density of moist air (CIPM-2007). *Metrologia* **2008**, *45*, 149. [CrossRef]
25. Lemmon, E.W.; Jacobsen, R.T.; Penoncello, S.G.; Friend, D.G. Thermodynamic properties of air and mixtures of nitrogen, argon, and oxygen from 60 to 2000 K at pressures to 2000 MPa. *J. Phys. Chem. Ref. Data* **2000**, *29*, 331–385. [CrossRef]
26. Mendoza, L.C.; Navarro-Esbrí, J.; Bruno, J.C.; Lemort, V.; Coronas, A. Characterization and modeling of a scroll expander with air and ammonia as working fluid. *Appl. Therm. Eng.* **2014**, *70*, 630–640. [CrossRef]